

Time Evolution of Relativistic Force-Free Fields Connecting a Neutron Star and its Disk

Eiji ASANO

Graduate School of Science and Technology, Chiba University,

1-33 Yayoi-cho, Inage-ku, Chiba 263-8522

asano@astro.s.chiba-u.ac.jp

Toshio UCHIDA

2-9-1-301, Shikatebukuro, Minami-ku, Saitama 336-0031

uchidat@jcom.home.ne.jp

and

Ryoji MATSUMOTO

Department of Physics, Faculty of Science, Chiba University,

1-33, Yayoi-cho, Inage-ku, Chiba 263-8522

matumoto@astro.s.chiba-u.ac.jp

(Received 2004 August 6; accepted 2005 February 16)

Abstract

We study the magnetic interaction between a neutron star and its disk by solving the time-dependent relativistic force-free equations. At the initial state, we assume that the dipole magnetic field of the neutron star connects the neutron star and its equatorial disk, which deeply enters into the magnetosphere of the neutron star. Magnetic fields are assumed to be frozen to the star and the disk. The rotation of the neutron star and the disk is imposed as boundary conditions. We apply Harten-Lax-van Leer (HLL) method to simulate the evolution of the star-disk system. We carry out simulations for (1) a disk inside the corotation radius, in which the disk rotates faster than the star, and (2) a disk outside the corotation radius, in which the neutron star rotates faster than the disk. Numerical results indicate that for both models, the magnetic field lines connecting the disk and the star inflate as they are twisted by the differential rotation between the disk and the star. When the twist angle exceeds π radian, the magnetic field lines expand with speed close to the light speed. This mechanism can be the origin of relativistic outflows observed in binaries containing a neutron star.

Key words: accretion, accretion disks—method: numerical—stars: magnetic fields—stars: winds,outflows

1. Introduction

Magnetic fields play essential roles in various activities observed in radio pulsars and in X-ray pulsars. In X-ray pulsars, an accretion disk surrounding a neutron star interacts with the magnetic field of the neutron star. In low mass X-ray binaries (LMXBs), angular momentum supplied from the accretion disk accelerates the rotation of the neutron star. These objects are sometimes observed as rejuvenated radio pulsars (e.g., Backer et al. 1982). Even in isolated radio pulsars, recent observations by the Chandra X-ray satellite (Weisskopf et al. 2000; Hester et al. 2002; Pavlov et al. 2003) revealed the existence of disk-like distribution of hot plasmas around the pulsar and the existence of bipolar jets. Magnetic interaction between the neutron star and its surrounding disk can be the origin of jet-like outflows.

The interaction between a magnetized star (neutron star, white dwarf or a young stellar object) and its accretion disk has been studied extensively. When magnetic field lines connect the star and its disk, their torque spins up or down the central star (e.g., Ghosh, Lamb 1978, 1979a, 1979b; Lovelace et al. 1995).

Zylstra (1988) obtained a sequence of twisted force-free fields around a neutron star and showed that when critical twist is accumulated, loss of equilibrium leads to the expansion of the magnetosphere. Lynden-Bell and Boily (1994) used semianalytic techniques for non-relativistic force-free configurations. By studying the evolution of force-free magnetic loops anchored to the star and the disk, they obtained self-similar solutions for it. They found that twist injection from the rotating disk makes the magnetic loops unstable and inflate and that the loops expand along the direction 60° from the rotational axis of the disk. Lovelace et al. (1995) applied this mechanism to keplerian disks.

In non-relativistic MHD case, Hayashi, Shibata, and Matsumoto (1996) carried out two-dimensional (axisymmetric) magnetohydrodynamic simulations of magnetic interaction between a star and its disk. They showed that magnetic reconnection takes place in the current sheet created inside the inflating magnetic loops. Their model can explain the X-ray flares and outflows observed in protostars. Miller and Stone (1997) presented the results of simulation including the rotation of the central star. Goodson et al. (1997, 1999) and Goodson and Winglee (1999) carried out longer time scale simulations of star-disk magnetic interaction and demonstrated quasi-periodic formation and destruction of magnetosphere by twist injection from the disk. Kato, Hayashi, and Matsumoto (2004) reported the results of MHD simulation of the magnetic interaction between a neutron star and its disk. They showed that due to the gas pressure external to the expanding loop, magnetic tower (Lynden-Bell 1996) is formed and that semi-relativistic jet flows out along the magnetic tower. This mechanism can explain the origin of semi-relativistic jets observed in Sco X-1 (Fomalont et al. 2001a, 2001b). In their simulation, however, special relativistic effects were neglected.

In magnetospheres of neutron stars, relativistic effects are not negligible. The purpose of

this paper is to extend the disk-star magnetic interaction model to a relativistic regime. When plasma density is low or magnetic field is strong, the Alfvén speed can be close to the light speed. Thus, we need to solve relativistic equations to study the evolution of the magnetosphere. Here we present numerical results for the magnetosphere dominated by the electromagnetic field, which can be described by time dependent relativistic force-free equations.

Recently, Komissarov (2002) carried out simulations of relativistic force-free fields to study the electrodynamics of pulsar magnetospheres and black holes. Here we extend the model for the case including a rotating equatorial disk threading the magnetosphere.

In section 2, we describe the force-free equations, numerical scheme, and redefinition of velocity fields. The results of simulations are given in section 3. Section 4 is devoted for summary and discussion.

2. Numerical models

2.1. Basic equations

We use force-free equations (e.g. Uchida 1997 for basic theory of force-free fields) derived from the special relativistic magnetohydrodynamics (SRMHD) equations to simulate the pulsar magnetosphere. The force-free approximation is applicable when the electromagnetic energy density is much larger than the energy density of the plasma. The force-free equations are

$$\frac{\partial \mathbf{P}}{\partial t} + \nabla \cdot \mathcal{M} = 0, \quad (1)$$

$$\frac{1}{c} \frac{\partial \mathbf{B}}{\partial t} + \nabla \times \mathbf{E} = 0, \quad (2)$$

where

$$\mathbf{P} = \frac{1}{4\pi c} \mathbf{E} \times \mathbf{B} \quad (3)$$

is momentum,

$$\mathcal{M}^{ij} = -\frac{1}{4\pi} \left[E^i E^j + B^i B^j - \frac{1}{2} \delta^{ij} (\mathbf{E} \cdot \mathbf{E} + \mathbf{B} \cdot \mathbf{B}) \right] \quad (4)$$

is electromagnetic stress tensor and c is speed of light. Equations (1), (2), (3) and (4) are equivalent to Maxwell's equations and the force-free condition,

$$\rho_e \mathbf{E} + \frac{1}{c} \mathbf{J} \times \mathbf{B} = 0, \quad (5)$$

where ρ_e is charge density and \mathbf{J} is current density. Equation (5) implies degeneracy of electromagnetic fields,

$$\mathbf{E} \cdot \mathbf{B} = 0, \quad (6)$$

which replaces the perfect conductivity condition in classical MHD (see Komissarov 2002). Under this condition, we can solve equation (3) as

$$\mathbf{E} = - \left(\frac{B^2}{4\pi c} \right)^{-1} \mathbf{P} \times \mathbf{B}. \quad (7)$$

We adopt \mathbf{P} and \mathbf{B} as fundamental variables for time dependent simulation. We normalize the equations by using the typical strength of magnetic field B_0 (on the surface of central star at rotational axis), and radius of the central star R_0 as units. The unit of time is $\tau_0 = R_0/c$. We use a spherical coordinate system (r, θ, ϕ) with $\theta = 0$ parallel to the star's rotational axis. We assume axisymmetry ($\partial/\partial\phi = 0$) but all three components of \mathbf{P} and \mathbf{B} are retained. We assume that the star's dipole moment is aligned with the rotational axis.

2.2. Definition of velocity fields

We introduce the velocity of magnetic field lines \mathbf{v}_B as

$$\mathbf{v}_B = \left(\frac{B^2}{4\pi c^2} \right)^{-1} \mathbf{P}. \quad (8)$$

This determines the velocity of the magnetic field lines uniquely. By using (8), the electric field \mathbf{E} is written as

$$\mathbf{E} = -\frac{1}{c} \mathbf{v}_B \times \mathbf{B}. \quad (9)$$

When the electric field is represented like equation (9), the electromagnetic field must satisfy

$$B^2 - E^2 \geq 0. \quad (10)$$

We checked that the condition (10) is satisfied throughout the calculation. Since the force-free equations are derived from the relativistic MHD equations by retaining the electromagnetic field only, plasma's velocity \mathbf{v} does not appear explicitly in the theory. However, we can assume the existence of the plasma that is frozen to the magnetic fields. If equation (10) is satisfied, the plasma can flow along the magnetic field lines.

2.3. Numerical scheme

We use the HLL method (Harten et al. 1983; Janhunen 2000) to solve the time dependent equations. It belongs to the family of an upwind scheme. In contrast to the Roe type scheme which requires eigenvalues and eigenvectors of the characteristic matrix, HLL scheme only needs eigenvalues. We used MUSCL-type method to attain second order accuracy in space. The HLL method is formulated as follows (Harten et al. 1983). A one dimensional hyperbolic system can be written in the form

$$\frac{\partial \mathbf{U}}{\partial t} + \frac{\partial \mathbf{F}}{\partial x} = \mathbf{S}, \quad (11)$$

where the vector of conservative variables is

$$\mathbf{U} = (P^i, B^i)^t, \quad (12)$$

$\mathbf{F} = \mathbf{F}(\mathbf{U})$ is the flux vector, and $\mathbf{S} = \mathbf{S}(x, t)$ is the source term. The fluxes are defined at cell interfaces. We denote the interface variables at the right- and left-hand side of each cell

interface as \mathbf{U}_R and \mathbf{U}_L . We denote the maximum speed of right- and left-going wave as b_R and b_L (in this simulation, $b_R = +c$ and $b_L = -c$) and the fluxes as $\mathbf{F}_R = \mathbf{F}(\mathbf{U}_R)$ and $\mathbf{F}_L = \mathbf{F}(\mathbf{U}_L)$. The HLL flux is then given by

$$\mathbf{F}_{\text{HLL}} = \frac{b_L \mathbf{F}_R + b_R \mathbf{F}_L - b_R b_L (\mathbf{U}_R - \mathbf{U}_L)}{b_R - b_L}. \quad (13)$$

Second order accuracy in time is achieved by first advancing \mathbf{U} by $\Delta t/2$ and next advancing \mathbf{U} by Δt using the flux at $\Delta t/2$.

We use 450 (model 1) and 460 (model 2) non-uniform grids in the radial direction and 180 uniform grids in θ -direction. The grid size is $\Delta r = 0.0125$ when $r < 1.125R_0$ and gradually increases as $\Delta r_{k+1}/\Delta r_k = 1.01$ when $r > 1.125R_0$. The maximum radius is $r_{\text{max}} = 100R_0$ (model 1) and $r_{\text{max}} = 110R_0$ (model 2).

2.4. Boundary conditions

We assume that dipole magnetic fields initially connect the central star and the geometrically thin disk at the equatorial plane ($3.0 \leq r \leq 95.0$). We assume that the central star and the disk are perfect conductors. At the equatorial plane, we impose boundary conditions such that B_r and B_ϕ are antisymmetric and B_θ is symmetric with respect to $\theta = \pi/2$. For electric fields, we impose the following conditions at $\theta = \pi/2$ ($3.0 \leq r \leq 95.0$),

$$\begin{cases} E_r = \frac{r\omega}{c} B_\theta, \\ E_\theta = -\frac{c r \omega}{c} B_r, \\ E_\phi = 0, \end{cases} \quad (14)$$

which imply that magnetic fields rotate with the disk. Here ω is the angular velocity of the Keplerian disk ($\omega = \sqrt{GM/r^3}$, where G and M are gravitational constant and mass of the central star, respectively). At the equatorial plane in $1.0 < r < 3.0$, we imposed the condition that E_r and E_ϕ are symmetric and E_θ is antisymmetric with respect to $\theta = \pi/2$. The magnetic field component B_θ at the equatorial plane is extrapolated from B_θ at the grid point next to the equator. The electric field E_r at the equator is computed by using equation (14). The momentum \mathbf{P} at the equator is computed by using equation (3) and (14).

The electric field on the stellar surface satisfies

$$\begin{cases} E_r = \frac{R_0 \Omega \sin \theta}{c} B_\theta, \\ E_\theta = -\frac{R_0 \Omega \sin \theta}{c} B_r, \\ E_\phi = 0, \end{cases} \quad (15)$$

where Ω is the angular velocity of the central star. The magnetic fields B_r , B_θ and B_ϕ at the stellar surface are extrapolated from B_r , B_θ and B_ϕ at the point next to the stellar surface. The electric field at the stellar surface is computed by using equation (15). The momentum \mathbf{P} is computed by using equation (3) and (15). In order to check that the footpoints of magnetic field

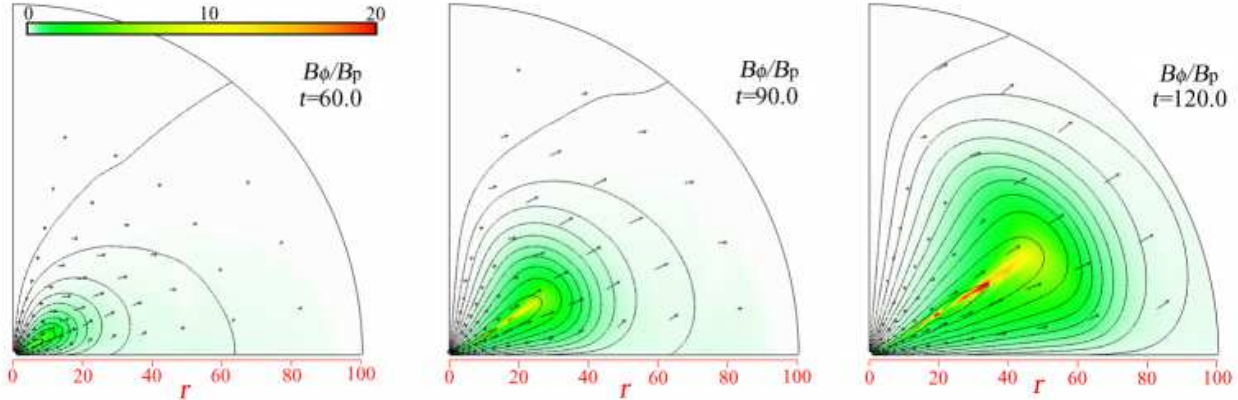


Fig. 1. Time evolution of magnetic field lines projected onto the $r - \theta$ plane (solid curves) in model 1. The color scale shows the twist B_ϕ/B_p . Arrows show the poloidal component of the velocity of magnetic field lines.

lines don't slip on the surface of the star and the disk, we computed the velocity of magnetic field lines near the surface of the star and the disk by using equation (8). We confirmed that \mathbf{v}_B coincides well with the rotational velocity of the accretion disk and the stellar surface.

We carried out simulations for two models. In model 1, we take $\Omega = 0$ and $\omega = 0.3(c/R_0)(r/R_0)^{-3/2}$. In model 2, we take $\Omega = 0.05c/R_0$ and $\omega = 0$. Model 2 corresponds to the disk far outside the corotational radius. We use free boundary conditions at the outer boundaries ($r = r_{max}$). On the rotational axis ($\theta = 0$), we substituted the values P_r and B_r at the grid point next to the rotational axis.

3. Numerical results

Results of simulations for model 1 are shown in figure 1. Solid curves in figure 1 show the magnetic field lines projected onto the $r-\theta$ plane. The color scale shows the strength of twist of magnetic field (B_ϕ/B_p) where B_ϕ is the toroidal magnetic field and B_p is the poloidal magnetic field. The arrows show the poloidal component of the velocity of magnetic field lines defined by equation (8).

The disk at $r = 3R_0$ rotates about 7 radian at $t = 120.0$. By the rotation of the disk, the magnetic field lines connecting the central star and the disk are twisted. Torsional Alfvén waves propagating along magnetic field lines are reflected on the surface of the central star. The typical crossing time of Alfvén waves travelling between the central star and the disk is $\sim 2r/c$. As time goes on, oscillations driven by the torsional Alfvén wave dissipates. Since the toroidal component of magnetic fields increases near the central star by accumulation of twist, magnetic pressure increases. From about $t = 50.0$, magnetic field lines begin to inflate. This rapid expansion of twisted magnetic loops takes place when the twist angle exceeds about π radian. The inflation is due to the loss of equilibrium in the twisted magnetic loops. Strong

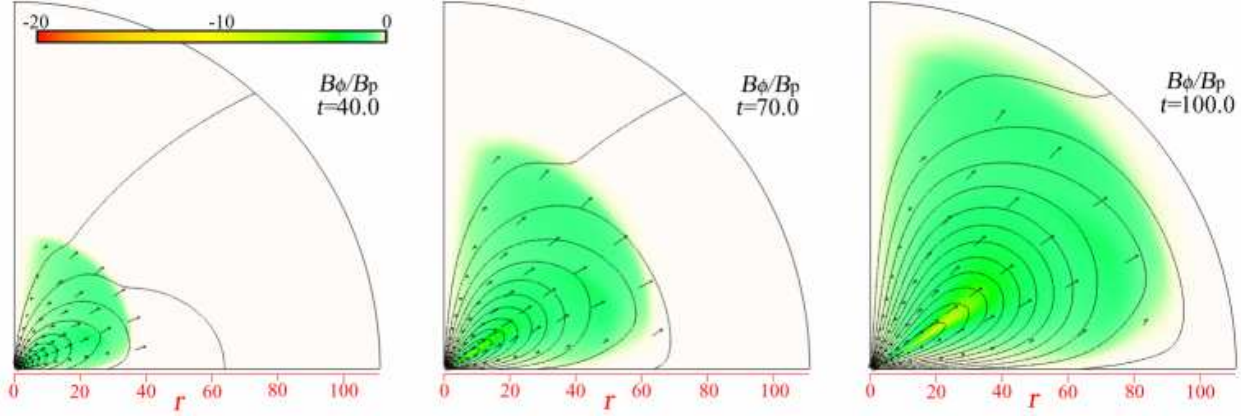


Fig. 2. The same as figure 1 but for model 2. Solid curves show magnetic field lines. Color scale shows the twist B_ϕ/B_p . Arrows show the poloidal component of the velocity of magnetic field lines.

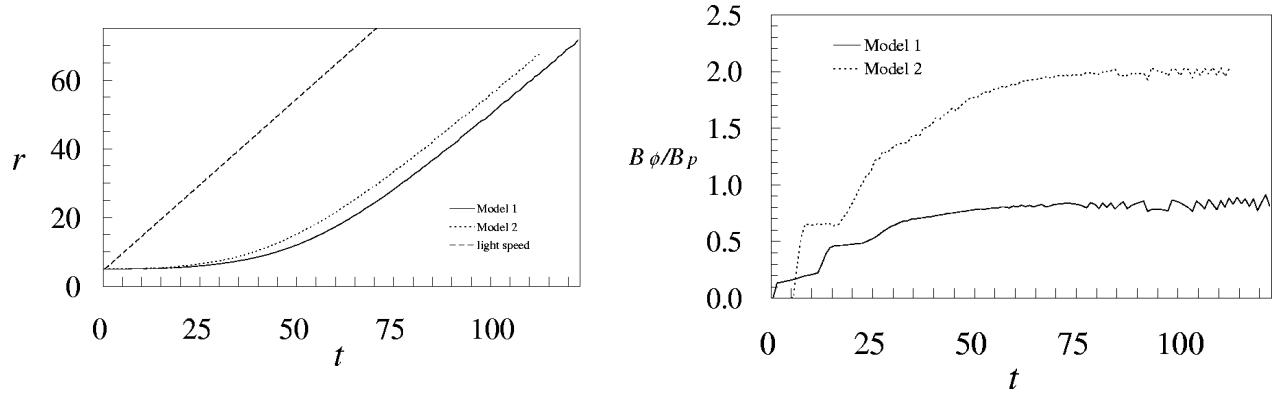


Fig. 3. (Left) Time evolution of the maximum distance from $r = 0$ to the point on the magnetic field line anchored to the disk at $r = 4.9$. The solid curve is for model 1 and the dotted curve is for model 2. The dashed line represents the wave propagating at light speed. (Right) Time evolution of the twist B_ϕ/B_p at the same point as that in the left figure. The solid curve is for model 1 and the dotted curve is for model 2.

current layer is created inside the expanding magnetic loops. These results are consistent with the stability analysis by van Ballegooijen (1994) and Lynden-Bell and Boily (1994). Figure 2 shows the time evolution of magnetic field lines (solid curves), twist (B_ϕ/B_p), and the poloidal component of the velocity of magnetic field lines (arrows) for model 2. In this model, the central star is rotating faster than the equatorial disk. Similarly to the model 1, the magnetic loops rapidly expand after $t = 50$ and form a long thin current sheet. The solid and dotted curves in figure 3 (left) show the maximum distance from $r = 0$ to the magnetic field line anchored to the equatorial disk at $r = 4.9$. The expansion speed approaches the light speed (dashed line). Figure 3 (right) shows the degree of twist (B_ϕ/B_p) at the same point as that of figure 3 (left). The twist increases with time until $t \sim 50$. Subsequently, the magnetic field lines inflate almost keeping the degree of twist. Figure 4 shows the poloidal velocity of the magnetic field line at

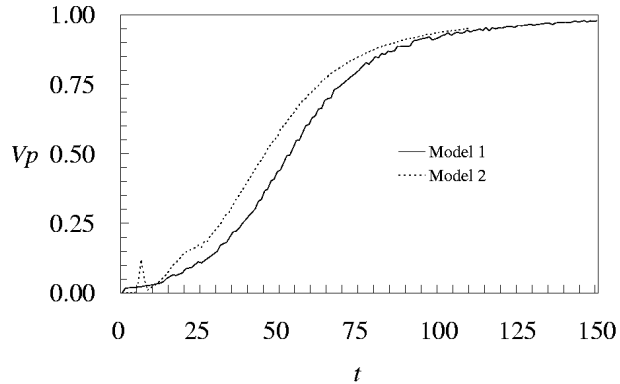


Fig. 4. The poloidal velocity of the magnetic field line at the same point as those depicted in figure 3. The velocity of magnetic field lines is defined by equation (8). The solid curve is for model 1 and the dotted curve is for model 2.

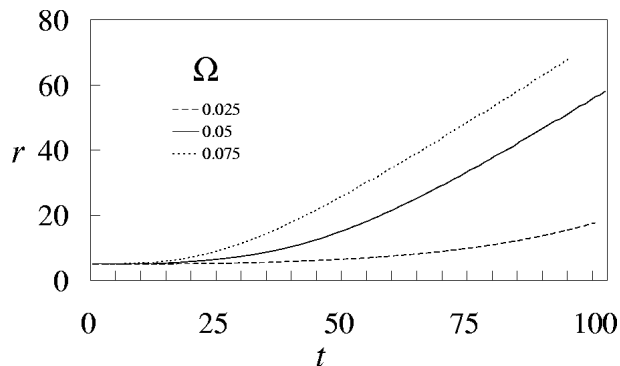


Fig. 5. The dependence of the radial expansion of magnetic fields on the angular speed of the central star, Ω , when $\omega = 0$ in the model 2. The curves show the maximum distance from $r = 0$ to the point on the magnetic field line anchored to the disk at $r = 4.9$. The solid curve is for model 2. The dotted curve is for $\Omega = 0.075$, and the dashed curve is for $\Omega = 0.025$.

the same point as those depicted in figure 3. The poloidal velocities in model 1 and 2 exceed 90% of the light speed at $t \sim 100$ and gradually approach the speed of light. Consequently, the toroidal velocity decreases and approach to zero.

Figure 5 shows the dependence of the radial expansion of magnetic fields on the angular speed of the central star, Ω , when $\omega = 0$. The solid curve is for model 2. As Ω increases, the poloidal component of the velocity of magnetic field lines approaches the light speed within shorter period.

4. Summary and Discussion

In this paper, we numerically solved the relativistic force-free degenerate electrodynamic equations to study the time evolution of magnetic field lines connecting a neutron star and its disk. This approach is an extension of the study by Uzdensky et al. (2002) in which they solved force-free magnetosphere by using semianalytic methods. Starting from potential magnetic

fields, we showed that magnetic fields are twisted by the differential rotation between the disk and the central star. After critical twist accumulates, the magnetic field lines connecting the star and the disk inflate with speed exceeding $0.95c$. In the region distant from the central star and the disk, the poloidal velocity approaches the speed of light. When the plasma is loaded to these expanding magnetic loops, we can expect relativistic outflows with Lorentz factor $\Gamma \geq 3$. A long thin current sheet is created inside these expanding magnetic loops. The elongation of the current sheet continues until the end of the calculation.

In this paper, we have solved ideal force-free equations. When the resistivity is included, magnetic reconnection will occur in the current sheet. Since force-free equations can't handle magnetic reconnection, we need to solve the full set of resistive MHD equations to simulate the magnetic reconnection. Another limitation of force-free approximation is that gas pressure does not appear in force-free equations. The existence of plasma pressure or magnetic fields helps collimating the expanding magnetic field lines toward the rotational axis (e.g. Kato et al. 2004; Tsinganos, Bogovalov 2002). Relativistic MHD simulations including gas pressure will be able to reproduce the collimated relativistic jets. We will report the results of such simulations in subsequent papers.

The authors thank Y. Uchida, S. Hirose, M. Nakamura for discussion. We thank S. Komissarov for discussion during the visit of R. Matsumoto to the University of Leeds. Numerical computations were carried out on VPP5000 at the Astronomical Data Analysis Center, ADAC, of the National Astronomical Observatory, Japan. This work is supported by the grant of ministry of education, science, sports, culture and technology (15037202, P.I. R. Matsumoto) and the Japan Society for the Promotion of Science Japan-UK Cooperation Science Program (P.I. K. Shibata and N. O. Weiss).

References

- Backer, D. C., Kulkarni, S. R., Heiles, C., Davis, M. M., & Goss, W. M. 1982, *Nature*, 300, 615
Fomalont, E. B., Geldzahler, B. J., & Bradshaw, C. F. 2001a, *ApJ*, 553, L27
Fomalont, E. B., Geldzahler, B. J., & Bradshaw, C. F. 2001b, *ApJ*, 558, 283
Ghosh, P., & Lamb, F. K. 1978, *ApJ*, 223, L83
Ghosh, P., & Lamb, F. K. 1979a, *ApJ*, 232, 259
Ghosh, P., & Lamb, F. K. 1979b, *ApJ*, 234, 296
Goodson, A. P., Böhm, K. H., & Winglee, R. M. 1999, *ApJ*, 524, 142
Goodson, A. P., & Winglee, R. M. 1999, *ApJ*, 524, 159
Goodson, A. P., Winglee, R. M., & Böhm, K. H. 1997, *ApJ*, 489, 199
Harten, A., Lax, P. D., & van Leer, B. 1983, *SIAM Rev.*, 25, 35
Hayashi, M. R., Shibata, K., & Matsumoto, R. 1996, *ApJ*, 468, L37

Hester, J. J., et al. 2002, ApJ, 577, L49
Janhunen, P. 2000, J.Comput.Phys., 160, 649
Kato, Y., Hayashi, M. R., & Matsumoto, R. 2004, ApJ, 600, 338
Komissarov, S. S. 2002, MNRAS, 336, 759
Lovelace, R. V. E., Romanova, M. M., & Bisnovatyi-Kogan, G. S. 1995, MNRAS, 275, 244
Lynden-Bell, D. 1996, MNRAS, 279, 389
Lynden-Bell, D., & Boily, C. 1994, MNRAS, 267, 146
Miller, K. A., Stone, J. M. 1997, ApJ, 489, 890
Pavlov, G. G., Teter, M. A., Kargaltsev, O., & Sanwal, D. 2003, ApJ, 591, 1157
Tsinganos, K., & Bogovalov, S. 2002, MNRAS, 337, 553
Uchida, T. 1997, Phys. Rev. E, 56, 2181
Uzdensky, D. A., Königl, A., & Litwin, C. 2002, ApJ, 565, 1191
van Ballegooijen, A. A. 1994, Space Sci. Rev., 68, 299
Weisskopf, M. C., et al. 2000, ApJ, 536, L81
Zylstra, G. J. 1988, Ph.D. thesis, Univ. Illinois, Urbana-Champaign